Received: 14 March 2022 | Revised: 25 November 2022 | Accepted: 25 November 2022

DOI: 10.1002/mrm.29559

RESEARCH ARTICLE

Magnetic Resonance in Medicine

A flexible 16-channel custom coil array for accelerated imaging of upper and infraglottic airway at 3 T

Wahidul Alam[1] | **Scott Reineke**[2] | **Madavan Raja Viswanath**[2] | **Rushdi Zahid Rusho**[1] | **Douglas Van Daele**[3] | **David Meyer**[4] | **Junjie Liu**[5] | **Sajan Goud Lingala**[1,6]

[1]Roy J. Carver Department of Biomedical Engineering, The University of Iowa, Iowa City, Iowa, USA

[2]ScanMed LLC, Omaha, Nebraska, USA

[3]Department of Otolaryngology, The University of Iowa, Iowa City, Iowa, USA

[4]Janette Ogg Voice Research Center, Shenandoah University, Winchester, Virginia, USA

[5]Department of Neurology, The University of Iowa, Iowa City, Iowa, USA

[6]Department of Radiology, The University of Iowa, Iowa City, Iowa, USA

Correspondence
Sajan Goud Lingala, Roy J. Carver Department of Biomedical Engineering, Department of Radiology, The University of Iowa, Iowa City, IA 52242, USA.
Email: sajangoud-lingala@uiowa.edu

Purpose: To develop a custom coil and evaluate its utility for accelerated upper and infraglottic airway MRI at 3 T.

Methods: A 16-channel flexible and anatomy-conforming coil was developed to provide localized sensitivity over upper and infraglottic airway regions of interest. Parallel-imaging capabilities were compared against existing head and head–neck coils. SENSE geometry factor losses were quantified for retrospectively accelerating 3D MRI. Blinded image-quality ratings from two experts were performed. Spiral GRAPPA reconstructions were evaluated for a speaking task at a time resolution of 40 ms. Contrast-to-noise ratios between air and tissue at key landmarks along the vocal tract were compared. SENSE imaging with the custom coil in the lateral recumbent posture was evaluated. Multislice imaging was performed to image swallowing at 17 ms/frame via constrained reconstruction.

Results: The custom coil showed improved SENSE imaging up to 3-fold acceleration when accelerated along either the anterior–posterior or the superior–inferior direction and a net 4-fold acceleration when accelerated along both directions. Spiral GRAPPA reconstructions with the custom coil showed higher contrast-to-noise ratio when compared with existing coils. In the lateral posture, robust SENSE imaging was achieved at up to 2-fold and 3-fold acceleration levels in the superior–inferior and anterior–posterior directions, respectively. Key events of swallowing in the multislice dynamic images were identified by an otolaryngologist.

Conclusion: The coil provided improved parallel imaging of upper and infraglottic airway in both supine and lateral recumbent postures. It enabled efficient accelerated dynamic imaging of speaking and swallowing.

KEYWORDS

custom coil, infraglottic airway, parallel MRI, upper-airway

1 | INTRODUCTION

The human upper airway consists of several structures such as the lips, tongue, hard palate, soft palate, larynx (including vocal folds), and pharynx, all of which coordinate with great dexterity to perform the essential day-to-day functions of speaking, swallowing, and breathing. MRI has emerged as a powerful modality to investigate the upper airway in applications such as assessing voice/speech disorders,[1] assessing airway collapse in sleep apnea,[2–4] understanding the mechanics of swallowing in normal subjects,[5] and assessing tongue cancer patients.[6] Imaging the infraglottic airway from just below the glottis until and including the upper trachea is crucial in understanding disorders such as subglottic stenosis[7] and tracheomalacia.[8] In voice production, the infraglottic vocal tract interacts acoustically with the supraglottic vocal tract during the open phase of phonation when the vocal folds are not closed. Imaging this part of the vocal tract thus enhances our understanding of vocal tract acoustics.[9,10] Inclusion of the infraglottic airway has also been shown to be crucial in computational fluid dynamic models that model air flow through collapsing airways as in obstructive sleep apnea and tracheomalacia.[11,12] Several upper and infraglottic airway MRI studies have relied on receive coils designed to image other body parts, such as the head-only coil, head-and-neck coil, and carotid coil.[2,7,13–16] Although these coils are useful, they are limited in their parallel-imaging performance due to the inferior diversity of the receiver coil sensitivity profiles in several important upper and infraglottic airway regions (e.g., soft palate, oropharynx, hypopharynx, base of tongue, vocal cords). Moreover, the widely available head and head–neck coils are typically rigid and bulky and can present challenges when it comes to (a) comfortably positioning patients with different face and neck geometries, (b) comfortably accommodating additional hardware, such as an air-flow face mask in sleep MRI studies, and (c) imaging in the lateral recumbent posture (e.g., during sleep). Two sites have demonstrated the value of custom coil arrays to accelerate upper airway MRI. These included lightweight designs of a 12-channel tongue coil at 3 T,[17] as well as 16-channel and 8-channel upper-airway coils at 3 T and 1.5 T, respectively.[18,19] Notably, the 8-channel coil at 1.5 T enabled a large linguistic study in which consistent image quality was reported across a range of subjects' face/neck geometries.[20] The lightweight and flexible nature of custom coils offers practical benefits such as (a) less sense of claustrophobia for subjects performing speech tasks during long protocols (often around 90 min[20,21]), and (b) ease of placing additional hardware such as a microphone to record speech/snoring or an air-flow mask to record expired CO_2 in sleep studies.

Motivated by the previous success of custom coil designs, we developed a novel 16-channel custom coil for accelerated imaging of the upper and infraglottic airway at 3 T. Our coil is lightweight and flexible and allows for imaging in both supine and lateral recumbent postures. We evaluated the parallel-imaging performance of our custom coil against a 48-channel head-only coil array and a 21-channel head–neck coil array. Through retrospective undersampling, we evaluated the capabilities of the coils to accelerate static 3D upper and infraglottic airway imaging via conventional SENSE reconstruction. Experiments on 3 volunteers with different face and neck sizes were performed. Data were evaluated in terms of quantitative geometry factor (g-factor) losses and qualitative scoring from two end-user experts (a vocologist/voice scientist and a sleep medicine physician). On one of the volunteers, performance of the custom coil in the lateral recumbent posture was established. The coils were compared to prospectively accelerate the task of dynamic vocal tract shaping during speech production using non-Cartesian (spiral) through-time GRAPPA reconstruction. Performance was assessed quantitatively in terms of the contrast-to-noise ratio (CNR) between various articulators and the air space in the vocal tract. Finally, the custom coil was used to image a normal volunteer swallowing a pineapple bolus oral contrast agent. Highly accelerated multislice dynamic imaging was performed via a sparse SENSE spiral spatiotemporal–constrained reconstruction scheme. The dynamics of swallowing were evaluated by an experienced otolaryngologist.

2 | METHODS

2.1 | Sixteen-channel custom coil design

The 16-channel coil was designed to provide localized sensitivity and variation of individual coil maps (i.e., spatial diversity) over the FOV spanning (a) the nasopharynx to the jugular notch of the sternum in the superior–inferior (SI) direction, (b) the tip of the nose to the posterior edge of the cervical vertebrae in the anterior–posterior (AP) direction, and (c) the left ear to the right ear in the left–right direction. The coil was constructed as three subgroups: the left cheek, right cheek, and chin and neck (Figure 1A). The left and right cheek groups had five elements each, and the chin and neck group had six elements. Each element group was separated into its own "paddle" to facilitate the best coil coupling to the subject anatomy for the largest possible variation of subject physique. Furthermore, the paddles also assisted in subject loading and unloading, as the paddles can be folded out of the way until the subject was in the desired position

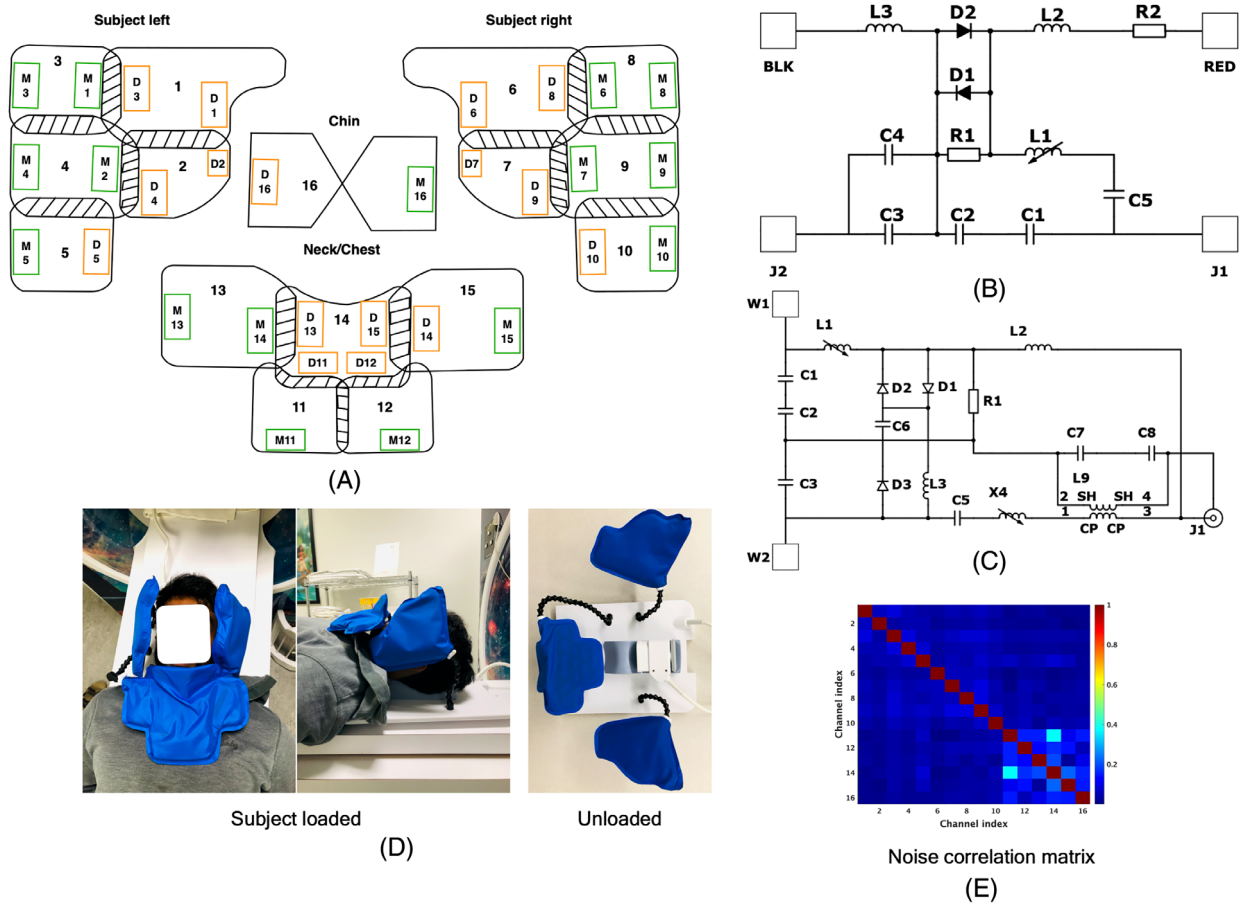

FIGURE 1 The 16-channel custom airway coil. A, As shown in the element layout, the coil was constructed as three pieces: two cheek pieces (with 5 elements each) and a neck+chin piece (with 5 + 1 elements). B,C, Schematics of the match board (orange boxes in [A]) and the decouple board (black boxes in [A]). D, The coil positioned on a representative volunteer. The flexible mounting of the pieces facilitates easy conformity to subjects with different sizes of face/neck geometry. E, Noise correlation matrix for the volunteer

on the patient table. Within every subgroup, individual antenna elements were overlapped (illustrated by gray "/" marks in Figure 1A) to minimize coil coupling. In addition, each element is attached to a low-input impedance preamplifier, further reducing coil-to-coil crosstalk. Each element had a passive decoupling junction to provide an additional layer of patient safety if an active decoupling junction were to fail (Figure 1B). In addition to a passive decoupling board, each element also had a match board. Each match board contained an active decouple junction, an impedance matching junction, and a cable trap (Figure 1C).

2.2 | IN VIVO EXPERIMENTS

2.2.1 | Static imaging: SENSE parallel imaging performance evaluation

The custom coil performance was compared with a 48-channel head-only coil and a 21-channel head-and-neck coil. For each of the coils, fully sampled 3D gradient-echo (GRE) data sets were acquired from 3 volunteers in the supine position in the resting posture on a GE SIGNA Premier 3T scanner. Before scanning, all volunteers signed informed consent forms approved by the University of Iowa's Institutional Review Board. Imaging parameters were TR/TE = 4.9/1.7 ms, flip angle = 5°, phase × frequency × slice partitions = 128 × 128 × 32, FOV = 24 × 24 × 6.4, voxel size = 1.9 × 1.9 × 2 mm, scan duration = 20 s, receiver bandwidth = 488.3 Hz/pixel, and readout in the SI direction. Raw data sets representing noise from each channel were also acquired using the same parameters, but with the flip angle set to 0°. The volunteers were chosen to represent size variations in head and neck anatomy and were labeled as large-head, medium-head, and small-head volunteers. The measured head volumes for these volunteers were $28 \times 22.4 \times 18\,cm^3$, $22 \times 19 \times 13\,cm^3$, and $21 \times 18 \times 9\,cm^3$ for the large-head, medium-head, and small-head volunteers, respectively. Measurements were made using the anatomical boundaries of the top of the

skull to the laryngeal prominence of the thyroid cartilage in the SI direction, the tip of the nose to the back of the skull in the AP direction, and the left ear to the right ear in the left–right direction. This FOV was prescribed so that the upper airway and infraglottic airspace were covered. We used the same imaging parameters with all study volunteers; therefore the anatomical coverage varied slightly between volunteers. On the large-head volunteer, imaging was performed in the lateral recumbent posture with the custom airway coil because comfortable subject positioning was not feasible with the head and head–neck coils.

Retrospective undersampling was performed along the subject's SI and AP directions for a range of reduction factors (R). One-dimensional (1D) undersampling was achieved by uniformly skipping every Rth k-space line along either the SI or the AP direction. Two-dimensional undersampling was achieved by uniformly skipping k-space lines by a factor of $R_{SI} \times R_{AP}$ along the SI and AP directions. Reduction factors ranging from 2-fold to 4-fold and from (2×2)–fold to (4×2)–fold were considered in 1D and 2D undersampling, respectively. The undersampled k-space data sets were subsequently reconstructed using 3D SENSE with no regularization. The sampling patterns always had the central 5% of the k-space to be fully sampled, which was used for coil-sensitivity estimation. The sum-of-squares approach was used to estimate the coil profiles. Before reconstruction, the raw k-space data were prewhitened by the knowledge of the noise covariance matrix.[22] For all of the undersampling settings with all of the coils, the g-factor maps were evaluated using the pseudo–multiple replica method[23] with 100 replicas. To better visualize differences among the reconstructions from the three coils, the pixel intensity in the reconstructed images was normalized with respect to the maximum intensity in the tongue region.

2.2.2 | Image-quality assessment by expert end users

To qualitatively assess image quality, these SENSE reconstructions were rated by two expert end users in a blinded manner (co-author J. Liu, a board-certified sleep medicine physician, and co-author D. Meyer, a vocologist and voice scientist). A total of 90 supine posture–based reconstructions spanning all coils, all undersampling factors, and all subjects were saved in the DICOM format. Similarly, a total of six lateral recumbent posture–based reconstructions across all undersampling factors from the single subject with the custom coil were saved. All of the images were randomized and presented to the raters in the open-source Horos software tool.[24] The raters could visualize the 3D reconstructions simultaneously in the sagittal, axial, and coronal cuts. Image quality in five anatomic regions were assessed using the following 4-point rubric:

- Score 1: Unacceptable quality. Strong noise and alias artifacts are present and hamper visualization of underlying anatomy.
- Score 2: Adequate quality. Moderate level of noise and alias artifacts and moderate level of interference with the visualization of underlying anatomy.
- Score 3: Good quality. Faint noise and artifacts are present but do not hamper visualization of underlying anatomy.
- Score 4: Excellent quality. Minimal to no noise and artifacts with clear visualization of underlying anatomy.

The anatomic regions chosen were (a) tongue, (b) velopharynx (airspace from the beginning of the velum to the end of the velum), (c) oropharynx (airspace from the end of the velum to the beginning of the epiglottis); (d) hypopharynx (airspace from the beginning of the epiglottis to the beginning of the larynx); and (e) infraglottic airway (airspace from just under the larynx to the end of the FOV in the inferior direction). In addition, raters were asked to provide a score in a sixth category of overall image quality. Figure S1 shows manual segmentation of these anatomic regions and an example format of the Horos interface presented to the raters. Nonparametric pairwise statistical comparisons of the scores were performed using the Kruskal–Wallis test. Comparisons were made between (a) the custom coil and the head coil, and (b) the custom coil and the head–neck coil.

2.2.3 | Dynamic imaging: Spiral GRAPPA parallel-imaging performance evaluation

On the large-head subject, we compared the performance of all three coils to prospectively accelerate dynamic imaging of speaking using spiral GRAPPA reconstruction. A 2D GRE-based, multishot, short-readout, uniform-density spiral sequence was implemented at a spatial resolution of 2.4 mm^2 and an FOV of 20 cm^2 (AP and SI directions) with a readout duration of 1.2 ms. Other relevant parameters were TR = 5 ms, flip angle = 5°, slice thickness = 6 mm, and midsagittal plane prescription. To satisfy Nyquist sampling, 34 spiral arms were required. Angular increments between successive spiral arms followed the golden angle of about 222.49°. The (k,t) sampling pattern was repeated with a periodicity of 34 interleaves. To calibrate the GRAPPA weights, data acquisition was performed using the same spiral sequence but with

the angular distribution sorted in an ascending order.[25] This was acquired for approximately 45 s, where the subject was counting numbers (verbally) at a comfortable pace. The subject was then instructed to perform the task of producing the phrase "za-na-za" in a repeated manner at a comfortable pace for 30 s, and (k–t) data were acquired using this golden-angle time-interleaved spiral sequence. For prospective undersampling, the raw (k–t) data were sorted using 8 arms/frame, 13 arms/frame, or 21 arms/frame, which corresponded to time resolutions of 40, 65, and 105 ms, respectively. Missing (k-t) samples for every channel were estimated using spiral GRAPPA. Inverse nonuniform Fourier transform reconstruction on the resulting output from spiral GRAPPA was performed. The final reconstruction was obtained after a root sum-of-squares coil combination of the reconstructions from the individual channels. Quantitative evaluation of the eight arms/frame reconstructions from the three coils was performed in terms of the CNR between the tongue and the airspace in the vocal tract at the following spatial landmarks: tongue tip, back of tongue, and base of tongue. The CNR was computed in 10 representative image frames during the production of the sound /a/ in /za/. A two-sample unequal-variance t-test statistic test was applied to compare the CNR between (a) the airway coil and the head coil and (b) the airway coil and the head–neck coil.

2.2.4 | Dynamic 2D multislice imaging of swallowing

The large-head subject swallowed approximately 10 ml bolus of pineapple juice, which served as a natural contrast agent due to the inherent presence of manganese. To capture the events during swallowing, a multislice, golden-angle, variable density–based spiral interleaved sequence was implemented (FOV = $20 \times 20\,cm^2$, spatial resolution = $2.4\,mm^2$, TR = 5.7 ms, readout duration = 1.2 ms, and three slices of thickness [6 mm, 1 midsagittal, 2 parasagittal]). Data were interleaved so that the spiral readout at the prescribed angle was acquired for all of the slices first before incrementing the angle. The raw data were sorted at one spiral arm per frame, which corresponded to an acceleration factor of about 27-fold with an effective time resolution of 17.1 ms/frame for the three slices. Regularized SENSE reconstruction was performed by exploiting sparsity of the dynamic time series under the spatiotemporal total variation transform in the BART (Berkeley Advanced Reconstruction Toolbox) computing environment.[26] The free regularization parameters were tuned empirically according to the L-surface decision rule on balancing the tradeoff between data consistency and regularization.[27,28] The spatiotemporal fidelity of the reconstruction was visually assessed in terms of identifying the key time events of a normal swallow. The analysis was performed by an expert otolaryngologist (coauthor D. Van Daele) who has 26 years of experience in clinical evaluation of swallowing disorders.

3 | RESULTS

Figure 2 shows a representative example of the individual 16-channel images with the custom coil in the midsagittal view from the fully sampled 3D-GRE data set on the large-head subject. The magnitude and phase of the coil sensitivity maps are also shown. The individual elements provide spatial sensitivity to the regions of interest, including the lips, tongue tip, tongue base, back of tongue, soft palate, pharynx, glottis, epiglottis, and infraglottic airspace. Furthermore, the individual elements are organized to provide spatial diversity (i.e., variation in coil sensitivity profiles) along the SI and AP directions. This is appreciated by the coil maps shown in Figure 2B,C.

Figure 3 shows the SENSE reconstructions and the associated g-factor maps from all three receive coils for R_{SI} between 2-fold and 4-fold for a representative large-head subject in the supine position. In comparison to the head-only and head–neck coils, the custom coil demonstrates graceful degradation in image quality with increased acceleration. For example, at $R_{SI} = 3$, in comparison to the airway coil, the head-only and head–neck coils depict noise amplification and artifact energy overlap on important soft-tissue structures such as the soft palate and tongue (see white arrows in Figure 3).

Figure 4 shows the subject's averaged g-factor maps at various acceleration combinations in the supine posture. The averaging of the g-factor maps was done over a region of interest focusing on the upper and infraglottic airway structures in the midsagittal plane (yellow mask in Figure 4). Notably, the airway coil in comparison to the head and head–neck coils provided (a) the fewest g-factor losses when accelerated along the SI directions for all subjects, and (b) comparable performance to the other two coils when accelerated in the AP directions for the large-head and small-head subjects. For the medium-head subject, the airway coil showed slightly greater average g-factor losses compared with the head–neck coil. When the subject was in the supine posture, the skewness in improved performance of the proposed coil in the SI direction was attributed to higher degree of spatial diversity in the coil elements along the SI direction compared with the AP direction.

Figure 5 shows combined image-quality ratings of the supine posture–based reconstructions. Score distribution

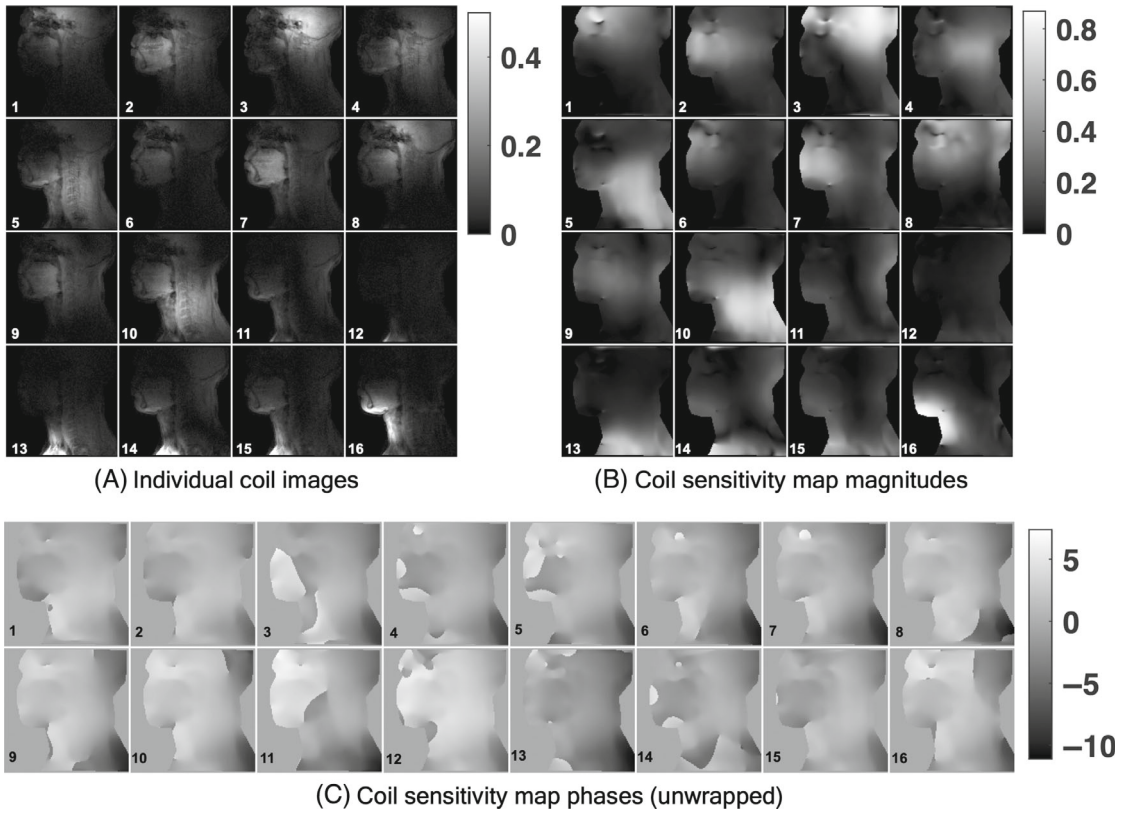

FIGURE 2 A, Individual coil images from the 16-channel elements. B,C, Magnitudes (B) and phases (C) of individual coil sensitivity maps for each of the channel elements. Coil sensitivities were estimated using root sum-of-squares methods from the central 5% of the k-space

for each coil and each acceleration setting is shown in a violin graph. Each violin graph consists of scores from 3 subjects and 2 raters. We mark the median score as a circle and the interquartile range as a black vertical box. The following results were observed:

- With 1D undersampling, by using a threshold cutoff score of median ≥ 3 (i.e., good image quality), we found the airway coil to provide acceptable quality up to $R_{SI} = 3$ and $R_{AP} = 3$ in all regions except for the hypopharynx region at $R_{AP} = 3$, which had a median score of 2.5;
- The airway coil provided consistently higher scores than the head-only coil up to $R_{SI} = 3$ and $R_{AP} = 3$. The Kruskal–Wallis pairwise comparisons showed differences in the categories of oropharynx, hypopharynx, infraglottic airway, and overall quality ($p \leq 0.2$; see orange asterisk);
- The airway coil provided similar scores to the head–neck coil at $R_{SI} = 2$ and $R_{AP} = 2$. However, at $R_{SI} = 3$ and $R_{AP} = 3$, the airway coil outperformed the head–neck coil. The Kruskal–Wallis pairwise comparisons showed differences in the categories of oropharynx, hypopharynx, infraglottic airway, and overall quality ($p \leq 0.2$; violet asterisk); and
- For both SI-direction and AP-direction undersampling (third row), using the cutoff criterion for good image quality (median score ≥ 3), we found that a net 4-fold ($R_{SI} \times R_{AP} = 2 \times 2$) acceleration was feasible with both the airway and head–neck coils. The airway and head–neck coils showed higher distribution of scores compared with the head coil in all categories. At this acceleration, the pairwise comparisons showed differences between the airway coil and the head-only coil in the categories of hypopharynx, infraglottic airway, and image quality ($p \leq 0.2$). Finally, the airway coil differed with the head–neck coil in the infraglottic airway category ($p \leq 0.2$).

Figure 6 shows SENSE parallel-imaging performance with the airway coil when the large-head subject was positioned in the lateral recumbent posture. We show reconstructions and associated g-factor maps at undersampling factors of 2-fold, 3-fold, and 4-fold. These are shown when undersampling was performed either along the subject's SI or the AP direction. We show representative axial cuts in the velopharynx and infraglottic air space regions. With 3-fold undersampling, the SI direction showed more pronounced noise amplification in the airway regions compared with the AP direction (see arrows). Both the SI and

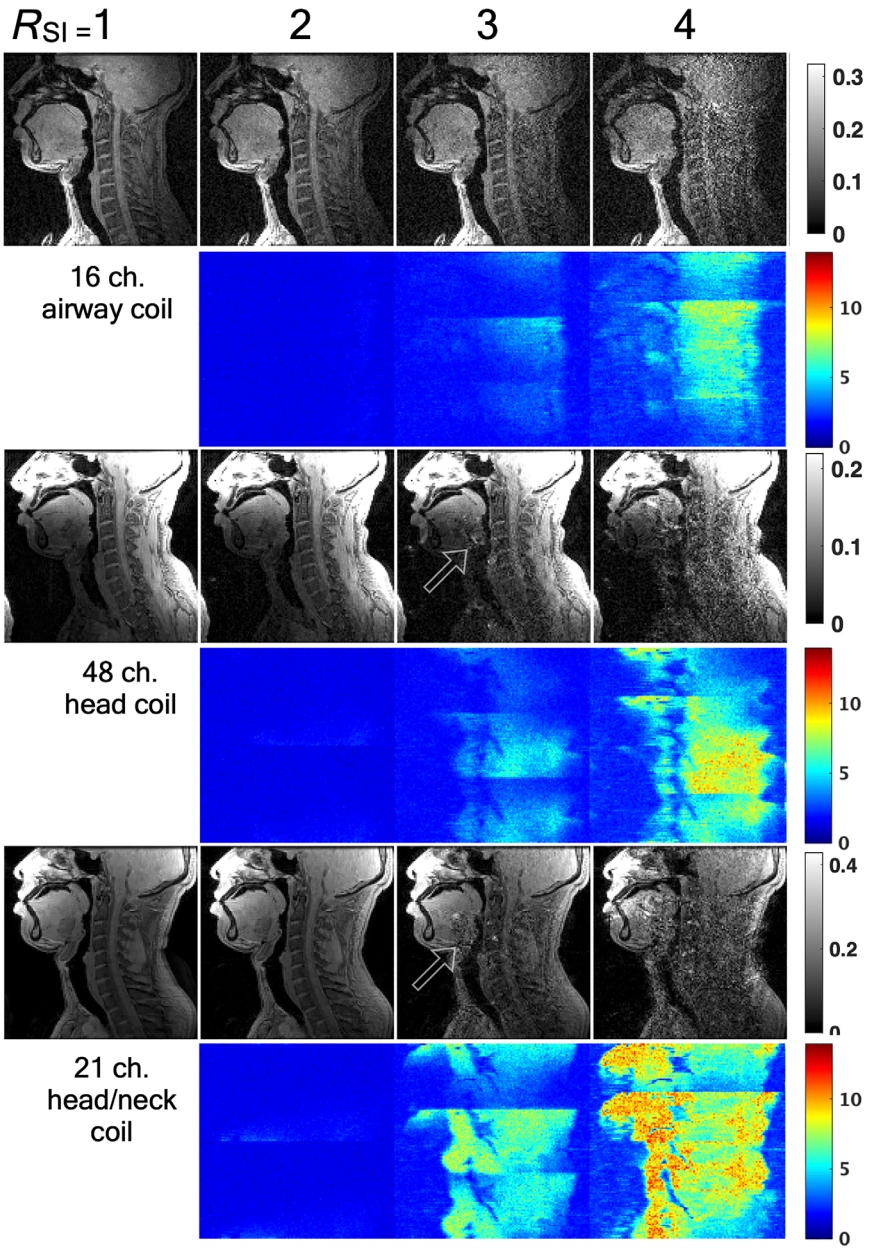

FIGURE 3 SENSE-based parallel MRI performance evaluations using retrospective one-dimensional (1D) undersampling on the large-head subject in the supine posture. SENSE reconstructions and associated g-factor maps are shown for the 16-channel airway coil, 48-channel head coil, and 21-channel head–neck coil at $R_{SI} = 1$-fold to 4-fold, respectively. The proposed coil demonstrates graceful degradation of image quality and g-factor losses when compared with the head and head–neck coils. In particular, even at $R_{SI} = 3$, we observe alias overlap and noise amplification in the oropharynx and hypopharynx regions with the head–neck and head coils. In contrast, the airway coil has a clearer depiction of these regions (see arrows)

AP directions produced poor quality at 4-fold undersampling.

Figure 7 shows the combined image-quality ratings for the lateral recumbent posture reconstructions. We observed consistently higher scores in all regions for ($R_{SI} = 2$)–fold and ($R_{AP} = 3$)–fold. A significant drop in scores was observed when R_{SI} was increased from 2-fold to 3-fold. However, the scores did not change significantly when R_{AP} was increased from 2-fold to 3-fold. With this cutoff for good image quality (median score ≥ 3), we found that $R_{SI} = 2$ and $R_{AP} = 3$ were feasible to image in the lateral posture for the large-head subject.

Figure 8 shows representative image frames from spiral GRAPPA reconstructions with all three coils at a time resolution of 40 ms/frame. The subject repeatedly produced the phrase "za-na-za." In comparison to the airway coil, both the head-only and head–neck coils showed a drop in contrast between vocal tract air space and soft-tissue regions. The head-only coil showed significant alias energy overlap onto the tongue and soft-palate regions. This compromised the interpretation of the dynamics of soft-palate closures against the pharyngeal wall during the production of the consonant sound /n/. In contrast, the head–neck coil and the airway coil qualitatively show good motion fidelity in capturing the articulatory movements.

Table 1 provides the quantitative comparison of spiral GRAPPA reconstructions in terms of CNR between the airspace in the vocal tract and the neighboring soft tissue at the spatial landmarks of the tongue tip, back of the tongue, and base of the tongue. The mean and SD

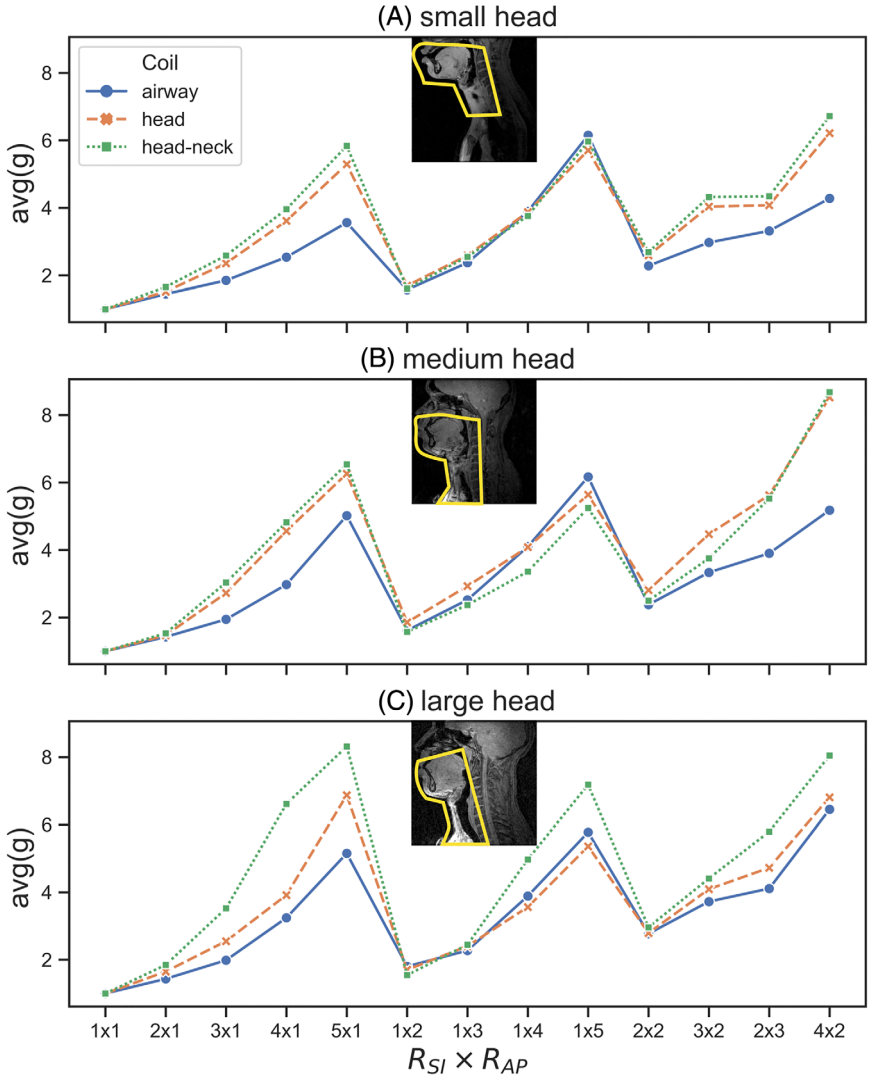

FIGURE 4 Averaged g-factor map comparisons between coils. The g-factor maps were averaged over the upper and infraglottic airway regions (see the yellow mask). Imaging was performed while the subjects were in the supine posture. With 1D undersampling, the average g-factor losses with the airway coil were the lowest when subsampled along the superior–inferior (SI) direction for all subjects and were comparable to the other coils when subsampled along the anterior–posterior (AP) direction for the large-head and small-head subjects. With 2D undersampling, the average g-factor losses with the airway coil were always lower when compared with the other coils

of CNR across the 10 frames are shown. The airway coil provided a significantly higher CNR compared with the head coil at all landmarks ($p \leq 0.001$). When compared with the head–neck coil, the airway coil provided a significantly higher CNR at the back of the tongue and the base of the tongue ($p \leq 0.001$). The airway coil's higher CNR throughout the vocal tract may provide images that can be used in intensity-based segmentation algorithms to better differentiate the articulators and the airspace.

Figure 9 shows a few image frames obtained from the swallowing experiment performed with the custom coil using prospective undersampling with a multislice spiral sparse SENSE scheme. Following inspection of the multislice (one midsagittal and two parasagittal) reconstructions as a video, the expert otolaryngologist (coauthor D. Van Daele) was able to delineate key events of the swallow (also marked in Figure 9). These were the events of oropharyngeal closure, velopharyngeal closure, laryngeal vestibular closure, upper esophageal sphincter opening, and laryngeal vestibular opening.

4 | DISCUSSION

In this investigation, a novel 16-channel flexible custom airway coil was developed, and its utility in upper airway and infraglottic airway MRI at 3 T was evaluated. In contrast to existing head and head–neck coils, the custom coil was constructed in a light-weight and flexible manner that adjusted to various face/neck anatomies, and permitted imaging in the lateral recumbent posture. We demonstrated improved SENSE parallel-imaging performance for the task of static 3D imaging of the upper airway and infraglottic airway. With blinded image-quality ratings from two experts, we found that in the supine posture, the custom coil enabled a net 3-fold acceleration when accelerated along either the SI or the AP direction and a net 4-fold acceleration when accelerated along both the SI and AP directions. Accelerated spiral GRAPPA reconstructions were achieved, which may allow for the dynamic imaging of speaking with a time resolution of 40 ms/frame. Real-time low-latency reconstructions using

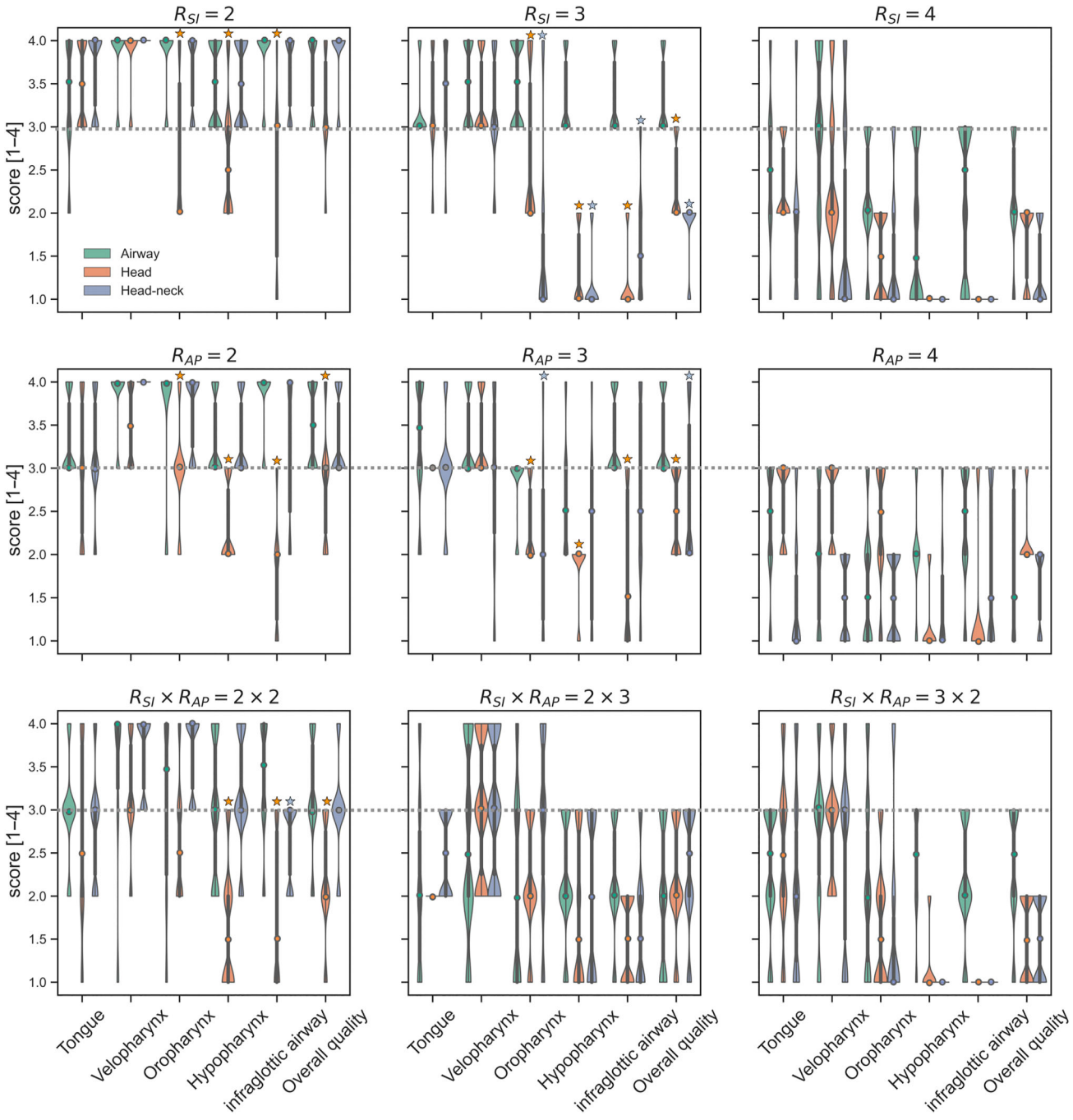

FIGURE 5 Blinded image-quality ratings of the supine posture–based reconstructions from two experts with experience in assessing airway geometry (a sleep medicine physician and a clinical voice scientist). Score distribution for each coil and each acceleration setting are displayed as a violin plot. Within each plot, the median is marked as a circle and the interquartile range as a black box. A dotted line is marked at the score = 3 (i.e., good image quality). With 1D undersampling in the SI or AP directions (first and second rows), in comparison with existing coils, we observed the proposed airway coil to consistently provide higher score distributions with a median score ≥ 3 in all categories up to 3-fold acceleration (except for the hypopharynx at $R_{AP} = 3$, where the median score was 2.5). With 2D undersampling (third row), both the airway and head–neck coils provided a median score ≥ 3 for a net 4-fold acceleration. The orange and violet asterisks indicate statistically significant ($p \leq 0.2$) pairwise differences between the airway (A) and head coils (B) and the airway and head–neck coils, respectively.

this technique may be possible in the future (e.g., biofeedback speech experiments, immediate inspection, assessment of swallow events). Finally, we showed highly accelerated imaging of a normal swallow event at a native time resolution of 17 ms/frame through a multislice spiral sparse SENSE scheme.

With the custom coil, we reported the preliminary feasibility of accelerated imaging in the lateral recumbent

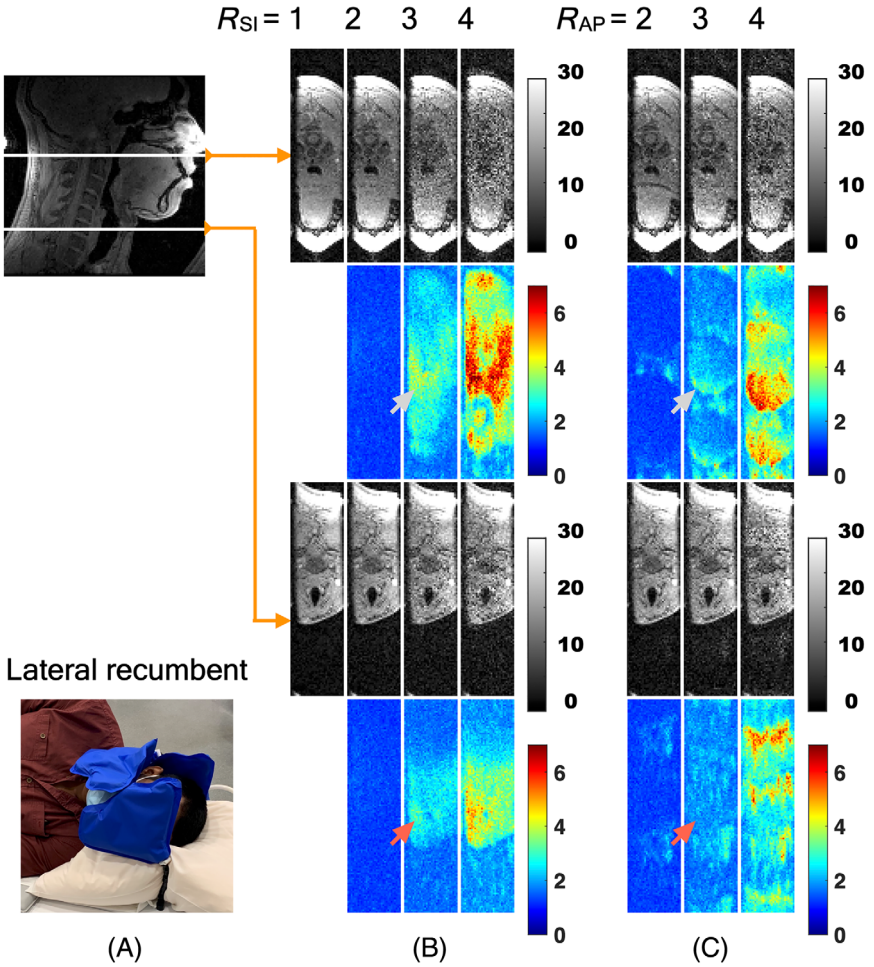

FIGURE 6 Demonstration of the custom coil in enabling upper and infraglottic airway imaging in the lateral recumbent posture. A, The flexible and lightweight nature of the arms of the coil allowed for easy positioning of the subject in the lateral recumbent posture. B,C, Representative axial cuts from the reconstruction and associated g-factor losses are shown in the velopharynx and infraglottic regions, respectively. We observed subtle improvements in the SENSE parallel-imaging performance when undersampling was performed in the AP direction compared with the SI direction. For instance, this is shown by more scattered g-factor noise patterns in ($R_{AP} = 3$)–fold reconstructions compared with more concentrated g-factor noise in the airway regions in ($R_{SI} = 3$)-fold reconstructions (also see corresponding arrows).

posture on a large-head subject. We found that 2-fold acceleration was feasible when accelerated along the SI direction and 3-fold acceleration was feasible when accelerated along the AP direction.

In the large-head subject, who had an oval-shaped head (i.e., narrower along the left–right direction), we note that the proximity of the left and right five-element cheek coil pieces were much closer to the deeper upper and infraglottic airway regions in the supine posture than in the lateral recumbent posture. Therefore, the sensitivity of the coil elements to upper and infraglottic airway structures was marginally lower in the lateral posture. However, in the lateral posture, we noted that the left and right cheek coil pieces conform to the front and back of the subject's head, thereby providing spatial diversity of the receiver coil profiles along the AP direction. This allowed for parallel imaging along this direction up to ($R_{AP} = 3$)–fold.

Previously, two sites had demonstrated the value of improved upper airway MRI using custom receive coils over generic head-only and head–neck coils. Our coil has some differences in the design criterion when compared with these existing custom coils. A key difference with our coil is its ability to provide higher sensitivity in the infraglottic airway region. The 12-channel design by Voskuilen et al.[17] focused on accelerated imaging of the tongue in swallowing MRI and diffusion MRI experiments. The coil elements were in physical contact with the subject's cheeks and chin. In contrast, our coil, and the coils used by Kim et al.[18] and Lingala et al.[19] do not touch the subject, as this could interfere with the natural movement of the jaw, chin, or lips during speech production. The 16-channel design used by Kim et al.[18] had a rigid design with closed-face encapsulation. Imaging subjects in the lateral recumbent posture with a coil of this design may be rather difficult. The design of upper airway coil elements as separate pieces facilitated by flexible paddles was first developed by Lingala et al.[19] at 1.5 T. A similar design was used in this paper. It should be noted that the imaging performance with flexible paddle-based coils may be susceptible to operator errors while coil positioning. This is a known limitation of this design, and a future test–retest repeatability study (such as in the work by Töger et al.[29]) is warranted.

A limitation of this work is the use of a small sample size in the evaluation of the coil. In this feasibility proof-of-concept work, we showed comparisons using

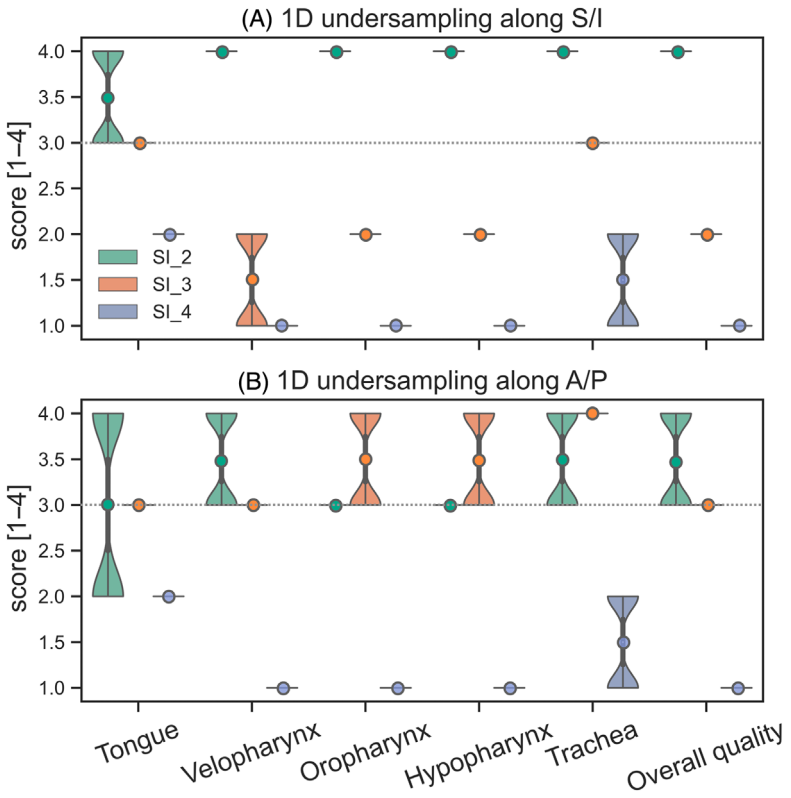

FIGURE 7 Blinded image-quality ratings of the lateral recumbent posture–based reconstructions via the airway coil on the large-head subject. Similar to Figure 5, we show the distribution of scores as a violin plot for different acceleration factors. When $R_{SI} = 2$, the median score was ≥3 in all of the categories. When R_{AP} was either 2-fold or 3-fold, the median score was ≥3 in all of the categories

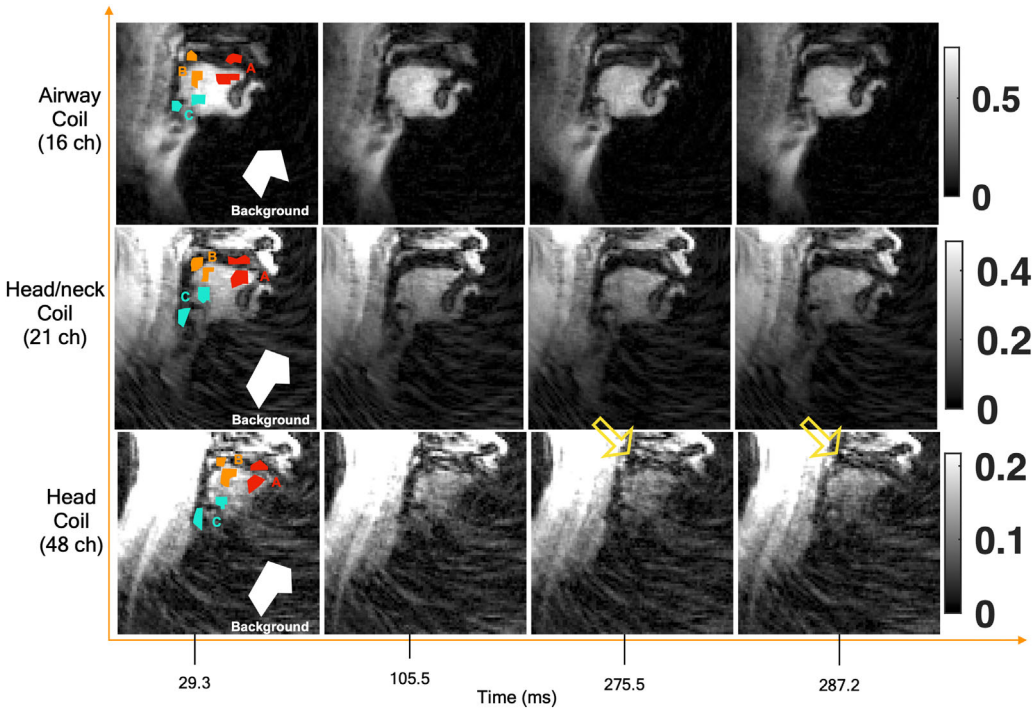

FIGURE 8 Spiral GRAPPA reconstruction for all three receive coils from prospectively undersampled data (eight spiral arms/frame, 2.4 mm^2, 40 ms/frame). The subject was instructed to repeat the phrase "za na za." Representative frames at different time instances are shown to depict vocal tract shaping during speech production. Regions A, B, and C marked in the first spatial frame were used to evaluate the contrast-to-noise ratio (CNR) between the soft tissue and vocal tract airspace in Table 1. The head-only coil shows significant residual alias energy overlap onto the soft palate (see yellow arrow). The head-only and head–neck coils depict low contrast between the vocal tract air space and surrounding soft-tissue articulators. In contrast, the airway coil provides superior contrast between the airspace and soft tissues. Both the airway and head–neck coils show good temporal fidelity in capturing the articulatory motion. (Video animation of this figure is provided in the Supporting Information)

TABLE 1 Comparison of CNR at three spatial landmarks along the vocal tract in spiral GRAPPA reconstructions

	Airway coil	Head coil	Head–neck coil
CNR_{tongue_tip} (A)	12.83 ± 2.74	7.22 ± 1.30	11.25 ± 2.70
CNR_{tongue_back} (B)	15.29 ± 2.32	10.31 ± 1.79	10.79 ± 2.02
CNR_{tongue_base} (C)	17.87 ± 2.91	8.25 ± 2.84	10.50 ± 2.45

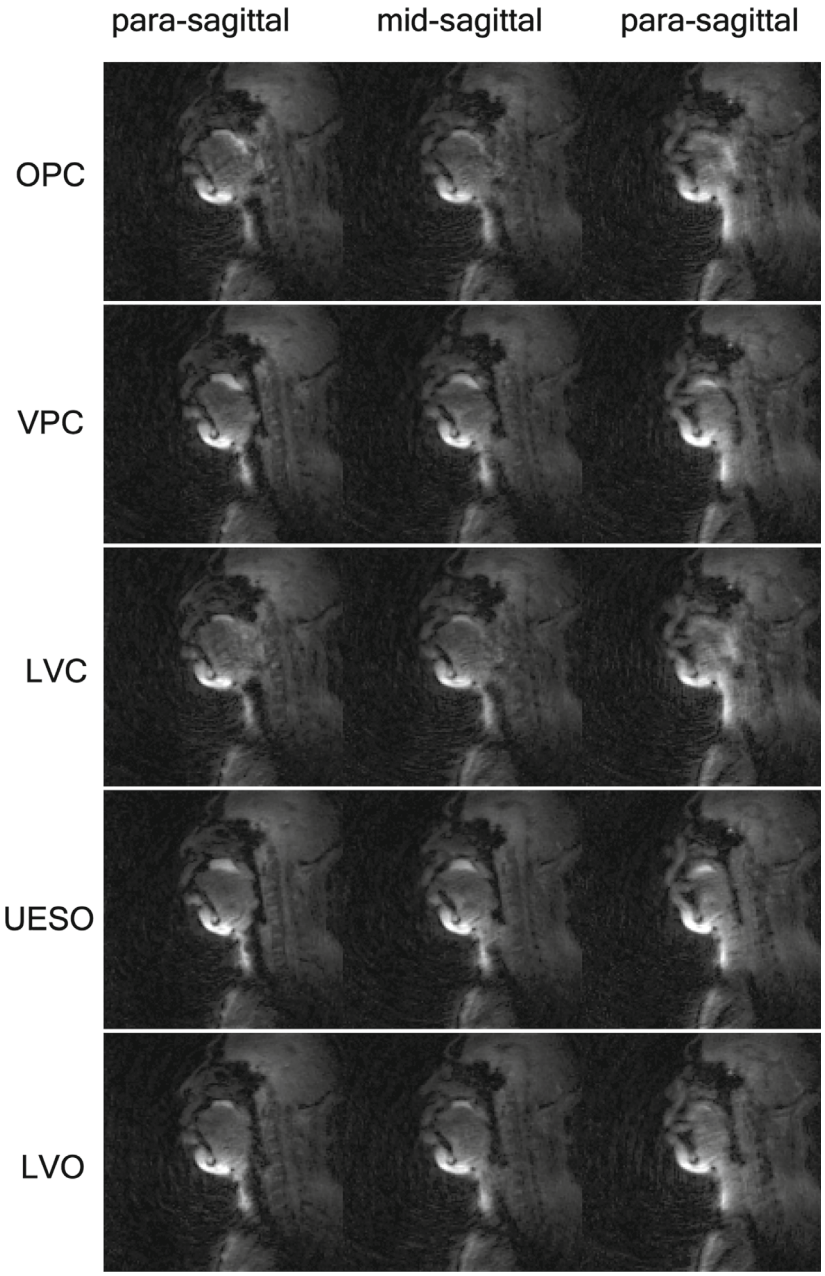

FIGURE 9 Demonstration of representative frames from 2D concurrent multislice accelerated dynamic imaging of swallowing an approximate 10-ml bolus of pineapple juice. Non-Cartesian spiral undersampling at approximately 27-fold acceleration level was combined with a sparse SENSE reconstruction scheme. The transport of the bolus (change of high-pixel intensity at the tongue tissue–air interfaces) is robustly captured in the three sagittal slices with adequate spatial resolution (2.4 mm^2) and temporal resolution (17.1 ms). (Video animation of this figure is provided in the Supporting Information.) Abbreviations: LVC, laryngeal vestibular closure; LVO, laryngeal vestibular opening; OPC, oropharyngeal closure; UESO, upper esophageal sphincter opening; VPC, velopharyngeal closure

only 1 volunteer each in the small-head, medium-head, and large-head categories in the SENSE-based comparisons. Our pair-wise nonparametric statistical comparisons were therefore established at a moderate *p*-value of ≤ 0.2. The spiral GRAPPA comparisons were done on 1 volunteer. Finally, the feasibility of swallowing and lateral recumbent posture imaging was shown on 1 volunteer. Future work with multiple subjects coupled with power analysis is needed to comprehensively establish the performance of the coil.

Off-resonance-induced blurring at air–tissue interfaces is a known limitation in using spirals for upper-airway

MRI. To reduce sensitivity to off-resonance, we implemented spirals using extremely short spiral readouts (~1.2 ms). Even with the short readout of 1.2 ms, we observed subtle air–tissue blurring on the tongue tip in the speaking data set. In future work, we will leverage dynamic field-estimation algorithms[30] to correct for such off-resonance artifacts.

With the custom coil, a nonuniformity of intensity distribution across several important regions of interest was observed. In particular, in the midsagittal orientation, the elements from the third neck/chin piece produced focal hyperintensities in the regions of the lips and chin due to their close proximity to these regions. This may limit immediate application of postprocessing schemes that operate based on pixel intensities. Future studies will address this using bias field-correction methods and correct for coil map–related intensity shading.

5 | CONCLUSIONS

The 16-channel flexible custom airway coil demonstrated improved SENSE parallel-imaging performance of up to 3-fold acceleration in both the superior–inferior and anterior–posterior directions when compared with the 48-channel head-only and 21-channel head–neck coils. The proposed coil is flexible and enabled imaging in both the supine and lateral recumbent postures. The coil demonstrated robust spiral GRAPPA reconstructions of dynamic speech imaging at a temporal resolution of 40 ms/frame. It showed improved CNR at various spatial landmarks along the vocal tract compared with existing coils. The coil enabled highly accelerated dynamic imaging of a swallow event at a native time resolution of about 17 ms/frame, where an expert otolaryngologist was able to delineate key swallow events.

ACKNOWLEDGMENT

This work was conducted on an MRI instrument funded by 1S10OD025025-01. We thank the Roy J. Carver Department of Biomedical Engineering, the Department of Radiology, and the Department of Otolaryngology at the University of Iowa for generously supporting the procurement of the custom coil. We gratefully acknowledge Melanie Laverman of the College of Engineering, and Deirdre Egan of the Writing Center at the University of Iowa for their assistance in proofreading and refining this paper.

CONFLICT OF INTEREST

Coauthors Scott Reineke and Madavan Raja were associated with Scan Med Inc., Nebraska, when building the custom coil reported in this work.

ORCID

Wahidul Alam https://orcid.org/0000-0003-0287-6690
Madavan Raja Viswanath https://orcid.org/0000-0001-8191-3546
Rushdi Zahid Rusho https://orcid.org/0000-0002-0963-1648

REFERENCES

1. Armour A, Fischbach S, Klaiman P, Fisher DM. Does velopharyngeal closure pattern affect the success of pharyngeal flap pharyngoplasty? *Plast Reconstr Surg*. 2005;115:45-52.
2. Welch KC, Foster GD, Ritter CT, et al. A novel volumetric magnetic resonance imaging paradigm to study upper airway anatomy. *Sleep*. 2002;25:530-540.
3. Moon IJ, Han DH, Kim J, et al. Sleep magnetic resonance imaging as a new diagnostic method in obstructive sleep apnea syndrome. *Laryngoscope*. 2010;120:2546-2554.
4. Chuang L-P, Chen N-H, Li H-Y, et al. Dynamic upper airway changes during sleep in patients with obstructive sleep apnea syndrome. *Acta Otolaryngol*. 2009;129:1474-1479.
5. Zhang S, Olthoff A, Frahm J. Real-time magnetic resonance imaging of normal swallowing. *J Magn Reson Imaging*. 2012;35:1372-1379.
6. Zu Y, Narayanan SS, Kim Y-C, et al. Evaluation of swallow function after tongue cancer treatment using real-time magnetic resonance imaging: a pilot study. *JAMA Otolaryngol Neck Surg*. 2013;139:1312-1319.
7. Henes FO, Laudien M, Linsenhoff L, et al. Accuracy of magnetic resonance imaging for grading of subglottic stenosis in patients with granulomatosis with polyangiitis: correlation with pulmonary function tests and laryngoscopy. *Arthritis Care Res (Hoboken)*. 2018;70:777-784.
8. Hysinger EB, Bates AJ, Higano NS, et al. Ultrashort echo-time MRI for the assessment of tracheomalacia in neonates. *Chest*. 2020;157:595-602.
9. Childers DG, Wong C-F. Measuring and modeling vocal source-tract interaction. *IEEE Trans Biomed Eng*. 1994;41:663-671.
10. Barney A, De Stefano A, Henrich N. The effect of glottal opening on the acoustic response of the vocal tract. *Acta Acust United with Acust*. 2007;93:1046-1056.
11. Bates AJ, Schuh A, McConnell K, et al. A novel method to generate dynamic boundary conditions for airway CFD by mapping upper airway movement with non-rigid registration of dynamic and static MRI. *Int j Numer Method Biomed Eng*. 2018;34:e3144.
12. Bates AJ, Schuh A, Amine-Eddine G, et al. Assessing the relationship between movement and airflow in the upper airway using computational fluid dynamics with motion determined from magnetic resonance imaging. *Clin Biomech*. 2019;66:88-96.
13. Schwab RJ, Kim C, Bagchi S, et al. Understanding the anatomic basis for obstructive sleep apnea syndrome in adolescents. *Am J Respir Crit Care Med*. 2015;191:1295-1309.
14. Kim Y, Lebel RM, Wu Z, Ward SLD, Khoo MCK, Nayak KS. Real-time 3D magnetic resonance imaging of the pharyngeal airway in sleep apnea. *Magn Reson Med*. 2014;71:1501-1510.

15. Okubo M, Suzuki M, Horiuchi A, et al. Morphologic analyses of mandible and upper airway soft tissue by MRI of patients with obstructive sleep apnea hypopnea syndrome. *Sleep.* 2006;29:909-915.
16. Shin LK, Holbrook AB, Capasso R, et al. Improved sleep MRI at 3 tesla in patients with obstructive sleep apnea. *J Magn Reson Imaging.* 2013;38:1261-1266.
17. Voskuilen L, de Heer P, van der Molen L, et al. A 12-channel flexible receiver coil for accelerated tongue imaging. *Magn Reson Mater Physics, Biol Med*. 2020;33:581-590.
18. Kim Y, Hayes CE, Narayanan SS, Nayak KS. Novel 16-channel receive coil array for accelerated upper airway MRI at 3 Tesla. *Magn Reson Med.* 2011;65:1711-1717.
19. Lingala SG, Zhu Y, Kim Y, Toutios A, Narayanan S, Nayak KS. A fast and flexible MRI system for the study of dynamic vocal tract shaping. *Magn Reson Med.* 2017;77:112-125.
20. Lim Y, Toutios A, Bliesener Y, et al. A multispeaker dataset of raw and reconstructed speech production real-time MRI video and 3D volumetric images. *Sci Data.* 2021;8:1-14.
21. Lingala SG, Toutios A, Töger J, et al. State-of-the-art MRI protocol for comprehensive assessment of vocal tract structure and function. In Proceedings of the 17th Annual Conference of the International Speech Communication Association, San Francisco, CA, 2016. pp. 475–479.
22. Hansen MS, Kellman P. Image reconstruction: an overview for clinicians. *J Magn Reson Imaging.* 2015;41:573-585.
23. Robson PM, Grant AK, Madhuranthakam AJ, Lattanzi R, Sodickson DK, McKenzie CA. Comprehensive quantification of signal-to-noise ratio and g-factor for image-based and k-space-based parallel imaging reconstructions. *Magn Reson Med.* 2008;60:895-907.
24. Horos™ (Horos Project, Geneva, Switzerland), an open source DICOM viewer for Mac OS X. Accessed May 2022. https://horosproject.org/
25. Lingala SG, Zhu Y, Lim Y, et al. Feasibility of through-time spiral generalized autocalibrating partial parallel acquisition for low latency accelerated real-time MRI of speech. *Magn Reson Med.* 2017;78:2275-2282.
26. Uecker M, Tamir JI, Ong F, Lustig M. The BART toolbox for computational magnetic resonance imaging. In Proceedings of the 24th Annual Meeting of ISMRM, Singapore, 2016;2486.
27. Hansen PC, O'Leary DP. The use of the L-curve in the regularization of discrete ill-posed problems. *SIAM J Sci Comput.* 1993;14:1487-1503.
28. Lingala SG, DiBella E, Adluru G, McGann C, Jacob M. Accelerating free breathing myocardial perfusion MRI using multi coil radial k− t SLR. *Phys Med Biol.* 2013;58:7309-7327.
29. Töger J, Sorensen T, Somandepalli K, et al. Test–retest repeatability of human speech biomarkers from static and real-time dynamic magnetic resonance imaging. *J Acoust Soc Am.* 2017;141:3323-3336.
30. Lim Y, Lingala SG, Narayanan SS, Nayak KS. Dynamic off-resonance correction for spiral real-time MRI of speech. *Magn Reson Med.* 2019;81:234-246.

SUPPORTING INFORMATION

Additional supporting information may be found in the online version of the article at the publisher's website.

Figure S1. Blinded image-quality ratings were performed by two expert raters by viewing the reconstructions in the Horos DICOM software. A screenshot of the interface simultaneously displays the sagittal, axial, and coronal cross sections. The regions of interest that were scored are marked in the sagittal plane

Figure S2. SENSE-based parallel MRI performance evaluations using retrospective 2D undersampling on the small-head subject in the supine position. Undersampling was done in the superior–inferior and anterior–posterior directions. For this subject, we qualitatively observe a much more graceful degradation of reconstruction with increasing acceleration level with the airway coil compared with the head and head–neck coils

Figure S3. SENSE-based parallel MRI performance evaluations using retrospective one-dimensional undersampling along the anterior–posterior (AP) direction on the large-head subject in the supine position. For AP direction undersampling in the supine posture for this subject, we qualitatively observe a similar level of degradation of image quality as acceleration is increased for all of the coils

Video S1. Spiral GRAPPA reconstructions of the speaking task at 40 ms/frame. The speech task was to produce repetitions of the phrase "za-na-za," which interleaves the /z/ and /n/ consonants with the /a/ vowel. Notice the good temporal fidelity of both the airway and head–neck coil in capturing the articulatory motion dynamics. The head coil shows poor representation of the velar motion due to unresolved aliasing. In comparison to the head-only and head–neck coils, the airway coil depicts higher contrast-to-noise ratio between soft tissue and vocal tract air space. Noise flickering in all of the reconstructions is due to spiral GRAPPA parallel imaging–related g-factor losses

Video S2. Concurrent multislice dynamic imaging of normal swallowing at 17 ms/frame. One midsagittal and two parasagittal slices were images. Images were reconstructed via a sparse SENSE spatiotemporal constrained reconstruction scheme. The dynamics of the moving pineapple bolus during swallowing are well captured by the proposed imaging scheme

How to cite this article: Alam W, Reineke S, Raja Viswanath M, et al. A flexible 16-channel custom coil array for accelerated imaging of upper and infraglottic airway at 3 T. *Magn Reson Med*. 2022;1-14. doi: 10.1002/mrm.29559